University of Tartu

Faculty of Science and Technology

Institute of Technology

Kirill Anohin

Development of Maximum Power Point Tracking for ESTCube-2

Bachelor thesis (12 EAP)

Computer engineering

Supervisors:

Janis Dalbins, M.Sc.Eng

Kristo Allaje, M.Sc.Eng

Tartu 2022

Abstract/Resümee

Development of Maximum Power Point Tracking for ESTCube-2

Maximum power point tracking is one of the most crucial components in a satellite. It allows for maximizing energy extraction from solar panels by varying the load of the solar cells for various environmental conditions. Without a functioning maximum power point tracking (MPPT), the CubeSat could experience power shortages that would eventually would lead to the shutdown of the entire system.

This thesis focuses on the creation of a Maximum Power Point Tracking system for the ESTCube-2 satellite. While there have been several Arduino based prototypes, none of them have actually been implemented on the final flight hardware and software. During the thesis, the author created a working prototype of the MPPT and implemented it with the satellite hardware. Furthermore, a set of tests were created and conducted in order to verify the work of the MPPT.

CERCS: T120 Systems engineering, computer technology; T170 Electronics; T320 Space technology

Keywords: CubeSat, ESTCube-2, Power harvesting

ESTCube-2 maksimaalse võimsuse jälgija arendus

Maksimaalse võimsuspunkti jälgimise süsteem (edaspidi MPPT) on satelliidi üks kõige tähtsamaid osi. See võimaldab päikesepaneelidelt võimalikult palju energiat kätte saada, muutes nende elektrilist koormust olenevalt väliskeskkonnast. Ilma töötava MPPT-ta võib kuupsatelliit kogeda elektrikatkestusi, mis võib põhjustada kogu satelliidi välja lülitumise.

Antud bakalaureusetöö keskendub MPPT süsteemi loomisele ESTCube-2 satelliidile. Varem oli loodud mõningaid prototüüpe Arduino baasil, kuid ühtegi neist poldud riist- ega tarkvaraliselt lõplikult implementeeritud. Lõputöö käigus lõi autor töötava MPPT prototüübi ja realiseeris selle satelliidi riistvaral. Autor lõi ja viis läbi erinevaid teste, et kontrollida MPPT tööd.

Contents

List of Figures

List of Tables

Acronyms

BCR Battery Charge Regulator. A device designed to limit the rate at which electric current is added to or drawn from batteries.. 27

CLI Command Line Interface. Interface that allows to communicate with the hardware via commands.. 36, 38

EPS Electrical power system. System designed to manage power within a spacecraft.. 6, 25–27, 29, 31

IC Integrated circuit. A chip or a small flat piece that contains a set of electronic circuits.. 31, 43

IncCond Incremental conductance. An MPPT algorithm that belongs to the "hill-climbing" group which uses conductance properties in order to find an MPP.. 6, 20–22, 25, 36

LEO Low Earth orbit. LEO is defined to be the distance of 2000km or less from the Earth's surface. 13, 30

MCU Microcontroller unit. Integrated circuit containing microprocessor along with memory and associated circuits. 20, 23, 25, 31, 32, 35, 36, 38, 41

MPB Main power bus. The primary power line of circuitry. 29, 42

MPP Maximum Power Point. The specific point on the current-voltage curve (I-V), where the solar array operates with maximum efficiency.. 15, 17–20, 22, 23, 25, 30, 37, 38, 41

MPPT Maximum power point tracking. Technique used with sources with variable power to maximize energy extraction under all conditions. 2, 3, 6, 8, 11–13, 17, 18, 23–27, 29, 31, 33–41, 43, 44

1 Introduction

Satellites consist of different complex systems that use electricity to operate. Therefore, satellites must have the ability to convert the energy around it into electrical energy locally. Commonly, the power harvesting system's primary power source is solar cells. Since solar cells produce a non-linear current-voltage relationship, a maximum power point tracking (MPPT) is required for efficient power extraction [1].

The MPPT uses current and voltage sensors to sample the solar array's power output and adjust the input operating voltage to match the point where the power output is at its maximum, allowing efficient power extraction from solar arrays. The excess power harvested from the primary power source should be accumulated in a storage device, most commonly, a battery pack.

The CubeSat standard was introduced to the world in 1999 as a collaborative effort between California Polytechnic University and Stanford University. The project's primary goal was to reduce developing time and cost of building a satellite and to increase accessibility to space for small companies and research institutes. The standard specifies that a one-unit CubeSat must have dimensions of 100 mm x 100 mm x 113.5 mm and should not exceed a mass of 2 kg. The CubeSat standard also supports scalability by one-unit increments. For example, a three-unit satellite can be made using the same cubic modules, giving maximum dimensions of 100 mm x 100 mm x 340.5 mm and a mass up to 6 kg [2].

ESTCube-2 is a three-unit successor to the one-unit ESTCube-1 CubeSat, developed by the Estonian Student Satellite Foundation and the Tartu Observatory, University of Tartu. Due to the addition of new experiments and subsystems, ESTCube-2 is larger and more ambitious than its predecessor. The mission aims to demonstrate a plasma brake deorbiting solution by deploying at least 30 m of conductive tether, potentially accelerating the mitigation of the space debris problem [3]. Among other payloads, the satellite will conduct a corrosion experiment developed by the University of Tartu, Institute of Physics, Laboratory of Thin Film Technology, and will carry two 5 megapixels Earth observation imagers that take images in different spectral

regions, made by Tartu Observatory.

This bachelor's thesis aims to test and integrate a MPPT system into the ESTCube-2 satellite. The thesis will give the reader a general overview of the working principles of an MPPT system in the chapter 2, along with showcasing other missions where an similar MPPT system was used and sets the requirements for ESTCube-2 MPPT development in chapter 3. Chapter 4 will provide the reader with detailed information about the developed MPPT algorithm, and the thesis will end by showcasing test results in chapter 5, followed by a conclusion where potential future improvements to the MPPT will be discussed.

2   Power harvesting in space

Power harvesting plays an important role in all forms of space explorations. Without a proper way to harvest power, a spacecraft can not maintain the needed electrical supply for the on-board systems.

The typical approach for most satellites is to use solar panels for power harvesting [4]. However, there are other methods of harvesting power in space such as radioisotope thermoelectric generator (RTG) and fuel cells [5],[6]. Typically, these systems are used in larger spacecraft far from the Sun, at distances where the light intensity becomes too low for practical solar panel deployment. Though they have not yet been integrated into CubeSats, the PocketRTG scientific development shows promising results for the future small satellite missions [7].

This thesis will focus on the most common method: harvesting power from solar cells which is also used by ESTCube-2 due to the readily available solar energy in low Earth orbit. The following sections provide the reader with a brief overview of the working principles of an MPPT functional block, along with an explanation of the most popular power tracking algorithms. The chapter ends with an examination of a few successful CubeSat missions that performed well in low Earth orbit (LEO). The chapter will focus on the techniques they used to maximize energy harvesting while in orbit.

2.1   Solar cell theory

A solar cell is a semiconductor device that converts visible and infrared light into electricity using the photovoltaic (PV) effect. The ideal solar cell model consists of the current source and a single diode connected in parallel. The output current from the current source is directly proportional to the emitted light from the light source. This ideal model is illustrated in figure 2.1 [8] where V represents the voltage across the output of the cell, I_{ph} is the photocurrent generated from the current source and I_d is the saturated current of the diode [9].
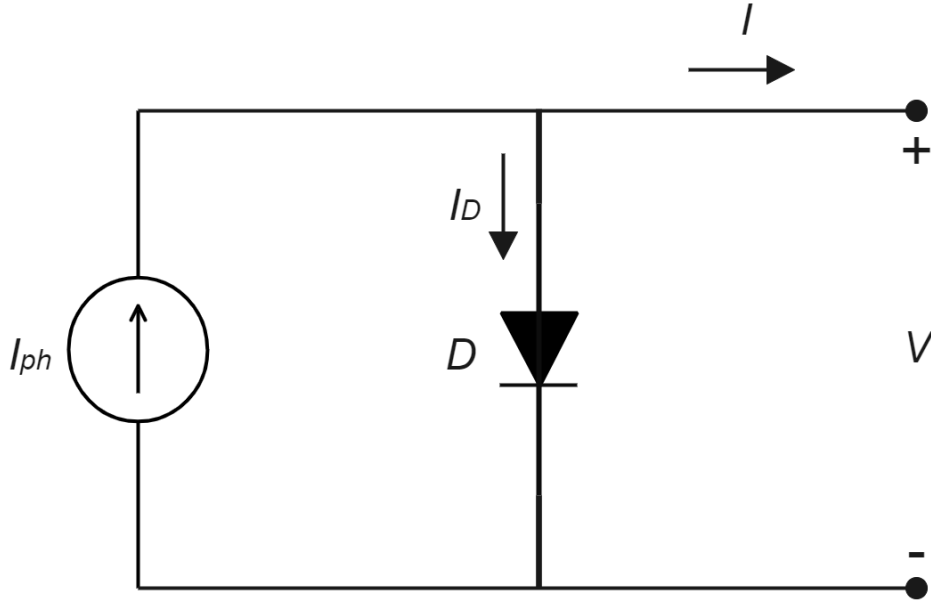
Figure 2.1. Equivalent circuit of an ideal PV cell.

The output current I of an ideal model of the solar cell can be shown as the relationship between I_{ph} and I_d:

$$I = I_{ph} - I_d \tag{2.1}$$

The current diverted through the diode can be expressed with the Shockley diode equation [9]:

$$I_d = I_S(e^{\frac{V_D}{V_T \cdot n}} - 1), \tag{2.2}$$

where I_d is the current through the diode, I_S is the reverse saturation current, V_D is the voltage across the diode, n is the diode ideality factor, and e is the Euler's number. V_T is the thermal voltage that can be calculated using $V_T = \frac{kT}{q}$ equation, where k is the Boltzmann constant, q is the charge of the electron, and T is the temperature in Kelvins.

By substituting 2.2 with 2.1 the expression of the ideal solar cell model 2.3 is achieved.

$$I = I_{ph} - I_S(e^{\frac{V_T}{V_T \cdot n}} - 1), \tag{2.3}$$

The more accurate and close to reality model can be introduced by adding shunt resistance R_{sh}, which accounts for the leakage current in the p-n junction, and series resistance R_s defining material resistivity. This equivalent circuit is shown in the diagram 2.2 [10].
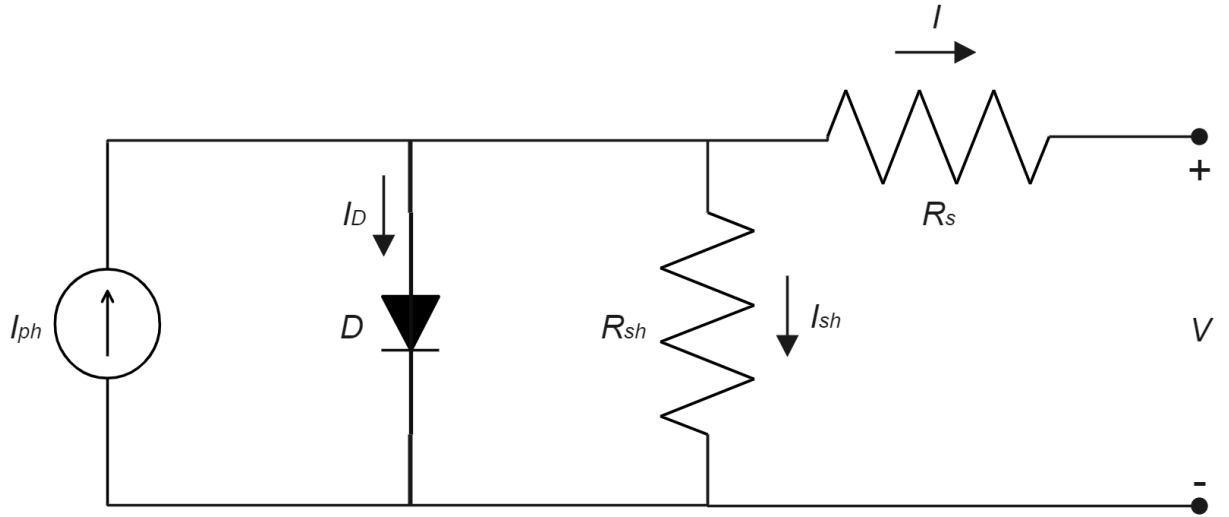
Figure 2.2. The equivalent circuit of a PV cell with serial and parallel resistance R_s and R_{sh}.

The relationship among additional parameters can be expressed as

$$I = I_{ph} - I_D - I_{sh} \tag{2.4}$$

where

$$I_d =_S \left(e^{\frac{(V+IR_s)}{V_T \cdot n}} - 1\right) \tag{2.5}$$

represent the diode current (I_d) incorporated with a series resistance (R_s), and

$$I_{sh} = \frac{(V + IR_s)}{R_{sh}} \tag{2.6}$$

is the current of shunt resistor (I_{sh}).

By substituting 2.5 and 2.6 with 2.4 equation is re-written as follows:

$$I = I_{ph} - I_S(e^{\frac{(V+IR_s)}{V_T \cdot n}} - 1) - \frac{(V + IR_s)}{R_{sh}} \tag{2.7}$$

2.2   Maximum Power Point Tracking

Solar cells have a non-linear current-voltage relationship, resulting in a specific point on the current-voltage (I-V) curve where they provide power with maximum efficiency. This point is called maximum power point (MPP) [10]. Another way to analyze the output efficiency is to use current-voltage (I-V), where the output of the solar cell is shown as a voltage with respect to current. The example of I-V and P-V curves created for AzurSpace 3G30A [11] cells using Matlab model with data available on the manufacturer's datasheet can be seen in the figures 2.3 and 2.4.
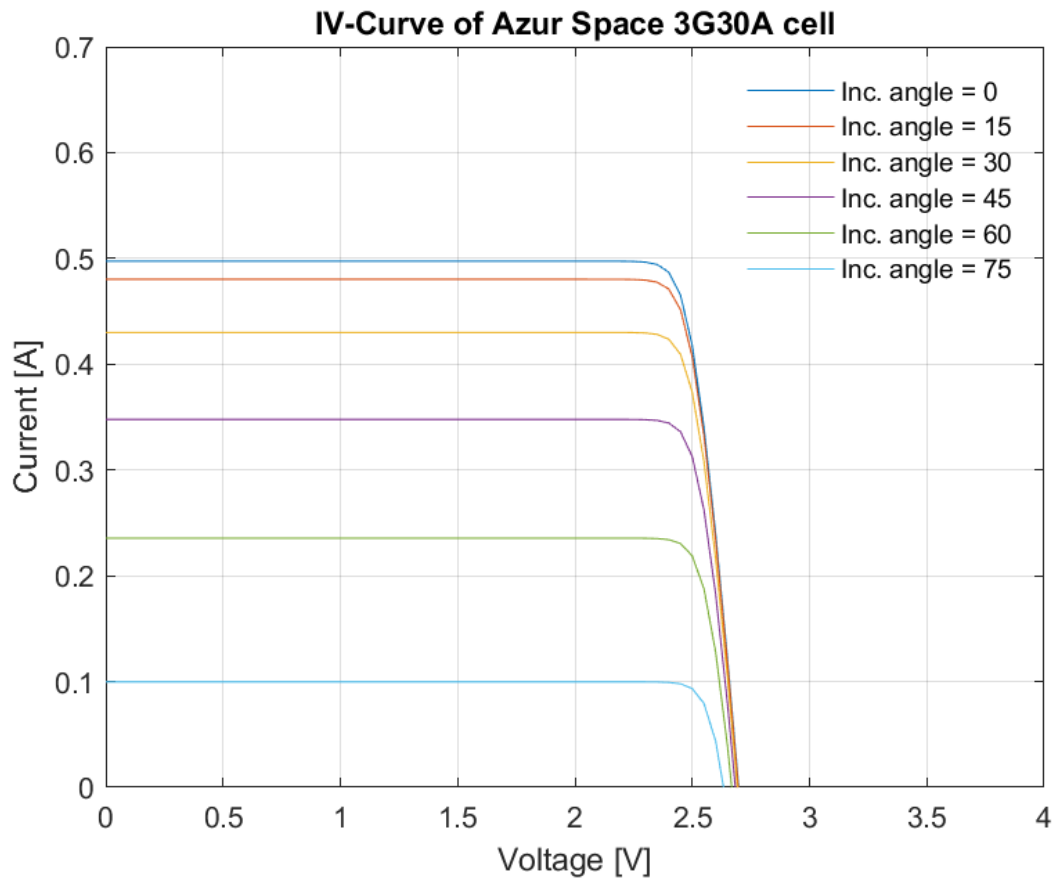
Figure 2.3. Simulated I-V curves of AzurSpace 3G30A cell at different angles of solar illumination.

The model was designed by Walker in 2001 [12] and was slightly modified in order to use with AzurSpace cells. The model uses a simplified model of solar cells resulting in series resistance and the recombination diode. A similar equivalent circuit can be seen in the figure 2.2.
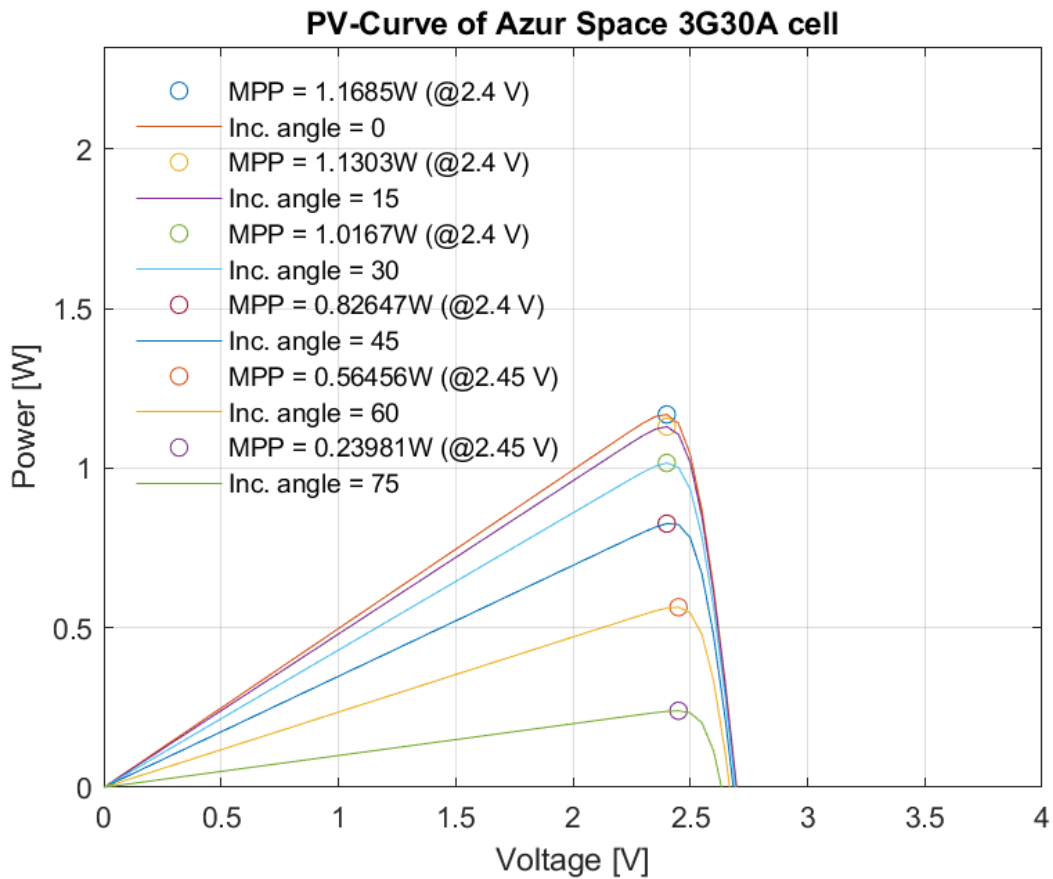
Figure 2.4. Simulated P-V curves of AzurSpace 3G30A cell at different angles of solar illumination.

The purpose of the MPPT is to keep the power harvesting circuitry operating at the point where the solar arrays can provide maximum power. The MPP location depends on multiple parameters such as solar irradiance, solar cell temperature, and degradation of solar cells. The I-V curves shown in figure 2.5 display how temperature changes the 3G30A solar cells' output characteristic. The figure shows that increasing temperature increases MPP current and decreases the voltage. Additionally, the voltage drops more rapidly than the current rises, which leads to a reduction in solar cell efficiency at higher temperatures. By comparing the I-V curves of 50°C and 28°C, the voltage drop in the power production of 3.8% is discovered while the current only increased by 1.2%.
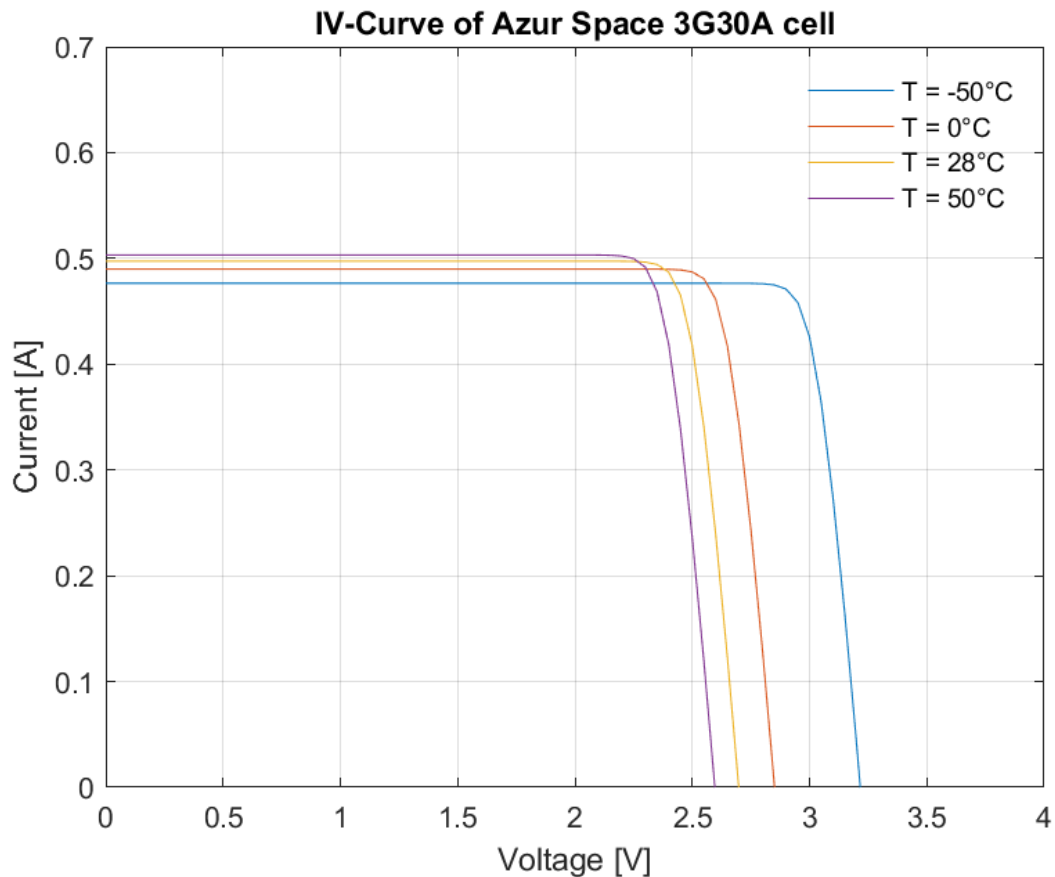
Figure 2.5. Simulated I-V curves of AzurSpace 3G30A in respect to temperature.

MPPT techniques used for locating the maximum power point can be classified into:

- Indirect methods - algorithms that rely on PV array characteristics. MPP is calculated with a simple assumption without measuring the power of PV arrays. Therefore, it is unreliable to use these methods to track the MPP precisely in space as the conditions such as temperature and irradiance will change rapidly [13].

- Direct methods - methods that will work under any condition as they process power, voltage, and current measurements of PV arrays to determine the exact location of the MPP.

A select number of implementable algorithms are presented below.

2.2.1 Perturb and observe

The perturb and observe (P&O) is the most widely used algorithm due to its simple implementation. The algorithm continuously measures the power from the solar array and raises or lowers the array voltage until the MPP is achieved. The main problem of this approach is that

the MPP can not be accurately determined with a large step size, generating steady oscillation around the MPP. On the other hand, a too small of a step size creates a considerable lag in the system and makes it less responsive to changes. Therefore there are modifications of the P&O algorithm that reduce the steady-state oscillations and to prevent the probability of tracking the MPP in the wrong direction under low power generation where the P-V curve of solar cell flattens [14],[1].

The following steps explain the behaviour of the P&O algorithm shown in diagram 2.6 [15].

1. Measure the input-voltage $V(k)$ and the input-current $I(k)$.

2. To acquire the initial power $P(k)$, calculate the product of $V(k)$ and $I(k)$.

3. Perturb the reference voltage of the solar panel V_{Ref} by a minimal step size in order to change the system operating point.

4. Compare current power reading $P(k)$ with the previously calculated $P(k-1)$.

5. If the harvested power level stays the same, the reference voltage will not be changed. Otherwise, the current-voltage $V(k)$ compared with the previous voltage $V(k-1)$ and the reference voltage is perturbed towards MPP.
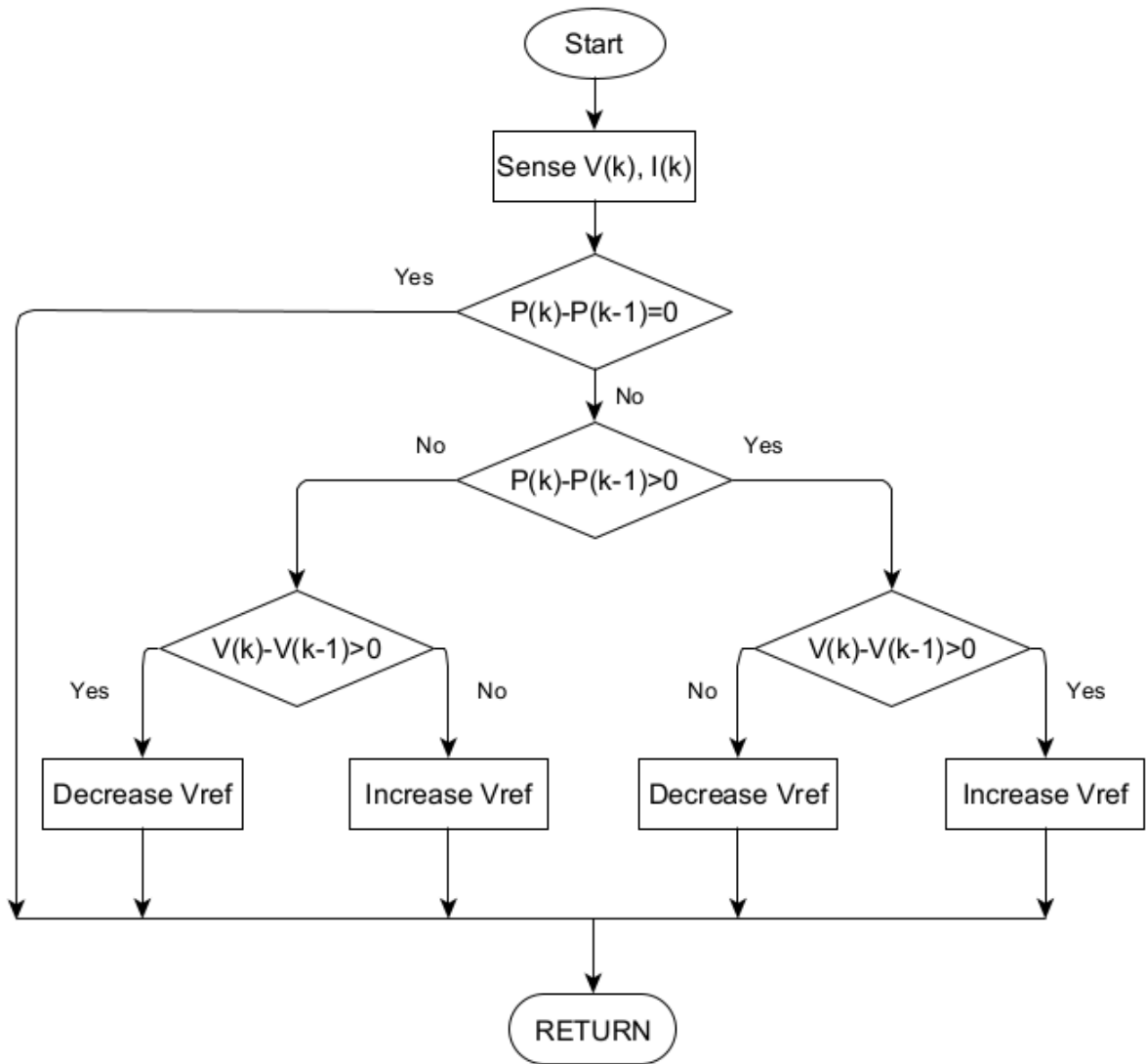
Figure 2.6. The flowchart of the P&O algorithm.

2.2.2 Incremental conductance

Electrical conductance determines how well an object can conduct electricity, and a similar name for this method is used because the algorithm compares incremental conductance $\left(\frac{\Delta I}{\Delta V}\right)$ with instantaneous conductance $\left(-\frac{I}{V}\right)$ and adjusts the reference voltage towards MPP. The main advantage of incremental conductance (IncCond) the algorithm is that it can accurately detect MPP direction. Compared to P&O algorithm, it decreases steady-state oscillation. However, the algorithm requires a relatively powerful microcontroller unit (MCU) capable of floating-point calculation due to the complex decision-making process, increasing overall system cost.

The MPP is achieved when eq. 2.8 is met.

$$\frac{\Delta I}{\Delta V} = -\frac{I}{V},\tag{2.8}$$

The increase in operating voltage of solar arrays happens when the incremental conductance is larger than the negative instantaneous conductance. Therefore, eq. 2.9 is met.

$$\frac{\Delta I}{\Delta V} > -\frac{I}{V} \qquad (2.9)$$

If the incremental conductance is smaller, the operating voltage is decreased. Therefore, eq. 2.10 is met.

$$\frac{\Delta I}{\Delta V} < -\frac{I}{V} \qquad (2.10)$$

The following steps explain the behaviour of the IncCond algorithm shown in the diagram 2.7 [15].

1. Measure the input-voltage $V(k)$ and the input-current $I(k)$.

2. If the change in PV array voltage remains stationary, the reference voltage V_{Ref} is increased or decreased by comparing the PV arrays current.

3. Otherwise, equations 2.8, 2.9, 2.10 are used to adjust the reference voltage accordingly.
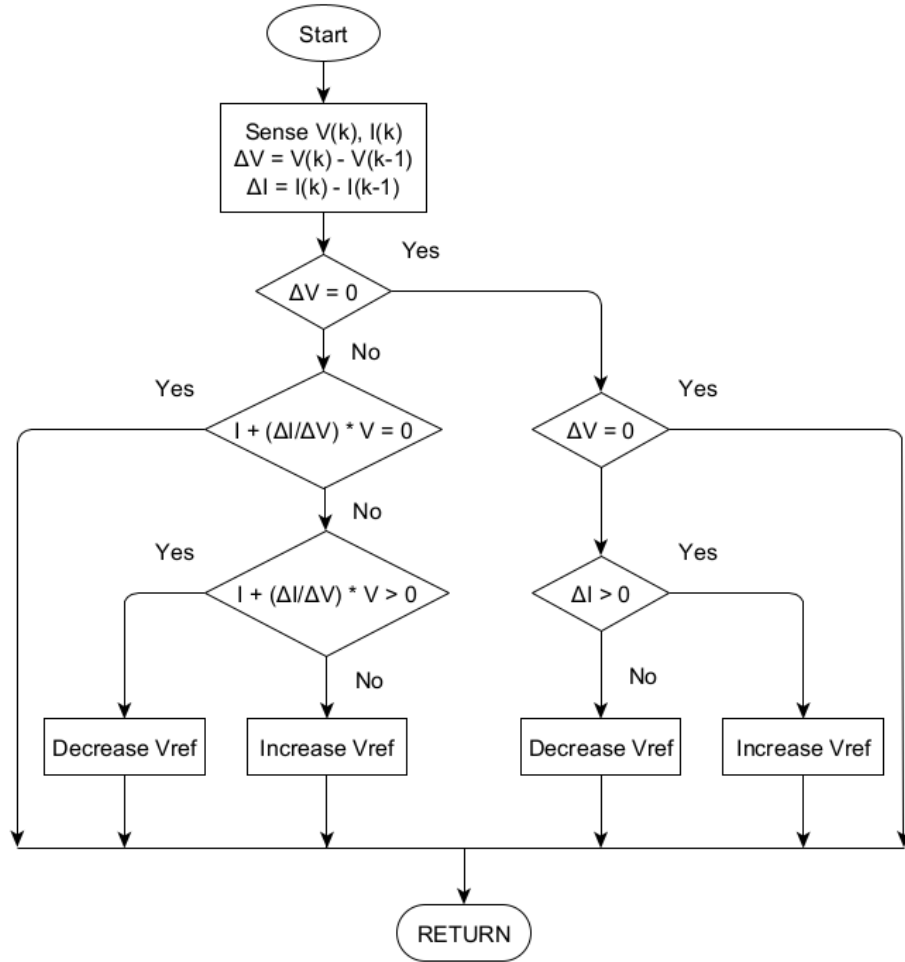
Figure 2.7. The flowchart of the IncCond algorithm.

2.2.3 Fractional methods

Both fractional open-circuit voltage and fractional short circuit current algorithms use the principle that the relation between V_{MPP} (or MPP current I_{MPP}) to the open-circuit voltage V_{OC} (or short circuit current I_{SC}) is almost linear. Therefore,

$$V_{MPP} = K_{OC}V_{OC}, \tag{2.11}$$

$$I_{MPP} = K_{SC}I_{SC} \tag{2.12}$$

where K_{OC} and K_{SC} are the constants that represent proportional gain [16]. The coefficients depend on factors such as parameters of PV elements and atmospheric conditions. Usually, K_{OC} has the interval of $[0.71, 0.78]$ and K_{SC} has $[0.78, 0.92]$ [14].

The main advantage of those techniques is that they can be implemented relatively quickly and require only a voltage or current sensor. However, the algorithms pose the problem of

needing open-circuit voltage/short-circuit current periodically measured, which interrupts the supply of power to the consumers [14].

2.2.4 Parasitic Capacitance

The parasitic capacitance (PC) algorithm is very similar to incremental conductance, with the main difference of taking into account the PV array parasitic junction capacity (PJC). PJC is caused by charge accumulation in the p-n junction area.

By including the parasitic capacitance C_p to the equation of the ideal solar cell (2.3), the following PV current equation is obtained:

$$I(t) = I_{ph} - I_S(e^{\frac{(V+IR_s)}{V_T n}} - 1) + I_c(t) = F(V_{PV}(t)) + C_p\dot{V}_{PV}(t),\tag{2.13}$$

where $I_c(t)$ represents capacitor current and is defined by equation 2.14.

$$I_c(t) = C_p\frac{dV_{PV}}{dt}\tag{2.14}$$

By taking derivative of multiplying equation 2.13 by PV array voltage the following equation of array power at MPP is obtained.

$$\frac{dF(V_{PV})(t)}{dV_{PV}(t)} + C\left(\frac{\ddot{V}_{PV}(t)}{\dot{V}_{PV}(t)} + \frac{\dot{V}_{PV}(t)}{V_{PV}(t)}\right) + \frac{F(V_{PV})(t)}{V_{PV}(t)} = 0,\tag{2.15}$$

where $\frac{dF(V_{PV})(t)}{dV_{PV}(t)}$ defined as incremental conductance and instantaneous conductance as $\frac{F(V_{PV})(t)}{V_{PV}(t)}$ of the PV array [17]. The dot represents the degree of the derivative.

2.2.5 Comparison of the different techniques

The review of different MPPT algorithms in the Nevzat Onat [18] article summarizes the performances, shown in table 2.1. As shown, Parasitic Capacitance, modified Perturb & Observe, and artificial intelligence-based algorithms show the highest power production efficiency. However, power production in CubeSats is sufficiently low. High-complexity algorithms such as artificial intelligence-based require a powerful MCU. Therefore, low-complexity algorithms are preferred due to lower power consumption and simpler design. Response time is also an essential factor that needs to be considered because of the rapidly changing environment, especially in space applications where the satellite's rotation can cause fast irradiance changes.

Comparison parameters	MPPT Algorithms					
	Perturb & observe	Modified P&O	Artificial intelligence	Constant voltage (current)	Incremental conductance	Parasitic capacity
Efficiency (%)	81.5–85	93–96	>95	88–89.9	73–85	99.8
PV Panel depending operation	No	No	Yes	Yes	No	No
Exactly MPP determination	Yes	Yes	Yes	No	Yes	Yes
Analog or digital control	Both	Digital	Both	Analog	Digital	Analog
Periodic tuning requirement	No	No	No	Yes	No	No
Convergence speed	Varies	Fast	Fast	Medium	Varies	Fast
Complexity	Low	Medium	High	Low	Medium	Low
Measured parameters	Voltage, current	Voltage, current	Varies	Voltage (current)	Voltage, current	Voltage, current

Table 2.1. Comparison of MPPT techniques.

The efficiency of MPPT algorithms was determined by:

$$\eta_{MPPT} = \frac{\int_0^t P_{MPPT}(t)dt}{\int_0^t P_{max}(t)dt},$$
(2.16)

where P_{MPPT} represents the power output of the PV system and P_{max} is the ideal MPP power output.

2.3 ESTCube-1

ESTCube-1 was a one-unit CubeSat that was equipped with twelve 3G30C triple-junction GaAs solar cells provided by AZUR SPACE Solar Power [11]. The solar cells were used as the primary energy source and they were placed in pairs on the spacecraft's six sides. However, because of the structure of the satellite, only three solar panels could be in direct sunlight at any given time, meaning that only those panels would provide power.

The electrical power system (EPS) design shown in diagram 2.8 consisted of three subsystems: power harvesting, distribution, and storage [19]. The energy harvesting system utilized a stand-alone SPV1040 MPPT IncCond that didn't require active control from the MCU. As at any given time only three power points needed to be tracked, due to the placement of the solar panels, three separate MPPTs were implemented.
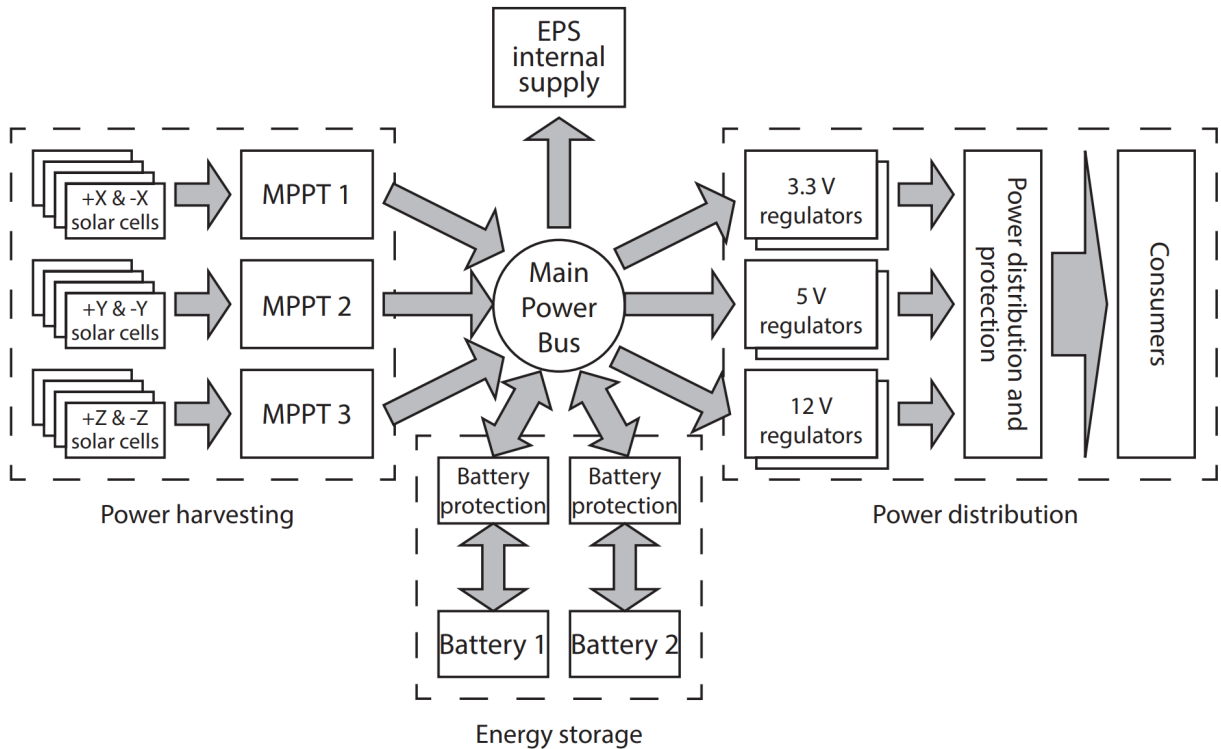
Figure 2.8. Diagram of EPS on ESTCube-1 satellite. Arrows show the flow of the energy.

The analysis of energy production showed the average power production under sun illumination of 2.2W at the beginning of the mission [20]. Unfortunately, the operation of the satellite's solar panels showed a degradation speed that was a lot faster than was anticipated. The reason for the problem is attributed to the lack of cover glass on solar cells allowing atomic oxygen or, possibly, radiation damage.

2.4 Qbx

The CubeSat Experiment or QbX was a three-unit spacecraft designed to explore a common nanosatellite platform for deployment of new technology at a faster rate and to reduce costs over traditional satellite platforms. The primary payload consisted of a custom-built Bus to Payload Interface Card, half-duplex TT&C radio, deployable dual-antenna, and a Low Rate Modem used for communication experiments.

The primary power source of the satellite consisted of 46 Emcore Advanced Triple-junction solar cells. The solar cells were placed on nine different panels (see figure 2.9): five body-mounted, and four deployable panels [21]. Each deployable and three body-mounted panels housed six solar cells, and the remaining two body-mounted had two cells per panel.
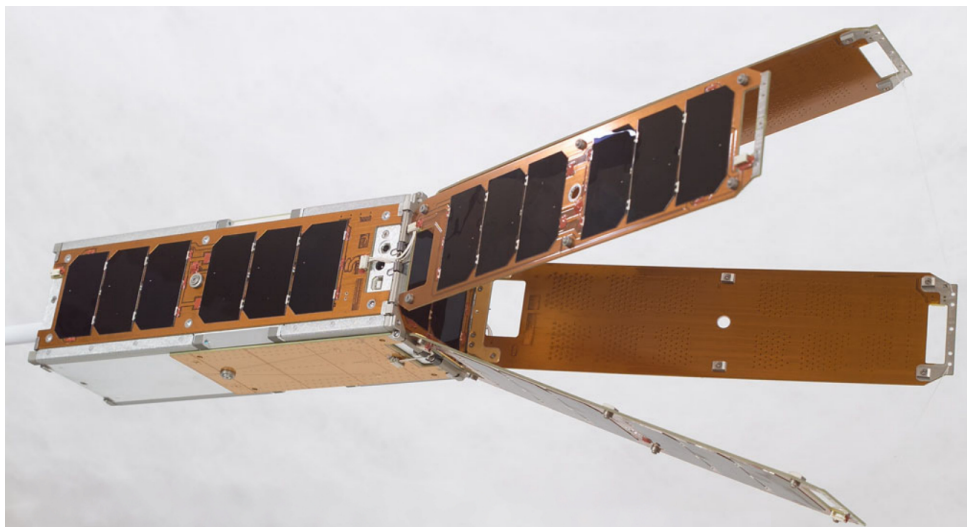
Figure 2.9. QbX CubeSat with its deployables open for maximum power harvesting.

The EPS was custom designed by Clyde Space and contained five independent MPPTs that worked autonomously. The solar panels with the arrangement of six cells were connected to MPPTs in pairs with a configuration that didn't allow for both panels to be illuminated simultaneously. Each MPPT converter could provide a maximum output of 8 watts of power. The remaining two cell solar panels were connected to the fifth MPPT, which was a single-ended primary-inductor converter, and it was able to output 5 watts of power. During the short mission

of QbX CubeSat, the MPPTs produced on average between 5.1 Watts to 8 Watts of power, as was intended. The electrical load was typically around 5 Watts, with the peak load of 15.5 Watts when the COM payload was enabled [22].

2.5   Aalto-1

Aalto-1 was a three-unit CubeSat initiated by the Department of Radio Sciences and Engineering of Aalto University. One of the mission's main goals was to test the electrostatic plasma brake designed by the Finnish Meteorological Institute.

The power harvesting system consisted of four solar panels located on the X and Y-axes of satellite. The -X and +Y side panels had the most solar cells per side, each panel containing eight cells. The remaining two panels -Y and +X had a lower amount of cells, six and two cells respectively, due to the placement of other subsystems. The generated power from solar panels was converted using three Battery Charge Regulators (BCRs) located on an EPS board provided by Clyde Space. The MPPT monitors kept track of the maximum power point and adjusted the BCRs to maintain the maximum power derived from the arrays. Each BCR operated independently from the others, meaning that if a failure event occured on one unit, the others would have continued to work [23].

The performance of the EPS was monitored using current, voltage, temperature sensors. The telemetry data revealed that the satellite's EPS was performing nominally, and required power was provided to satellite subsystems. However, degraded performance of one solar panel, shown by the green plot in figure 2.10, was discovered. The cause of the problem is unknown [24].

Figure 2.10. Captured intensities of current generated by solar panels starting from launch date until Aug 2019.

3 ESTCube-2 power distribution overview

The ESTCube-2 power distribution network aims to provide power to all subsystems and to protect the supplied systems from excessive current consumption. The structure of the satellite's power distribution network can be seen in the figure 3.1 [25].

The main part responsible for managing the satellite's power is the EPS mainboard. The EPS is connected to other parts of the distribution network via the main power bus (MPB) bus, which has a floating voltage from 6.6 V to 8.4 V. The current on the MPB lines can flow bidirectionally between the side panels, EPS mainboard and battery management board. The rest subsystems and payloads can only receive power from the EPS mainboard. Additionally, the EPS provides 3.3 V and 5 V power lines for the satellite subsystems and payloads.
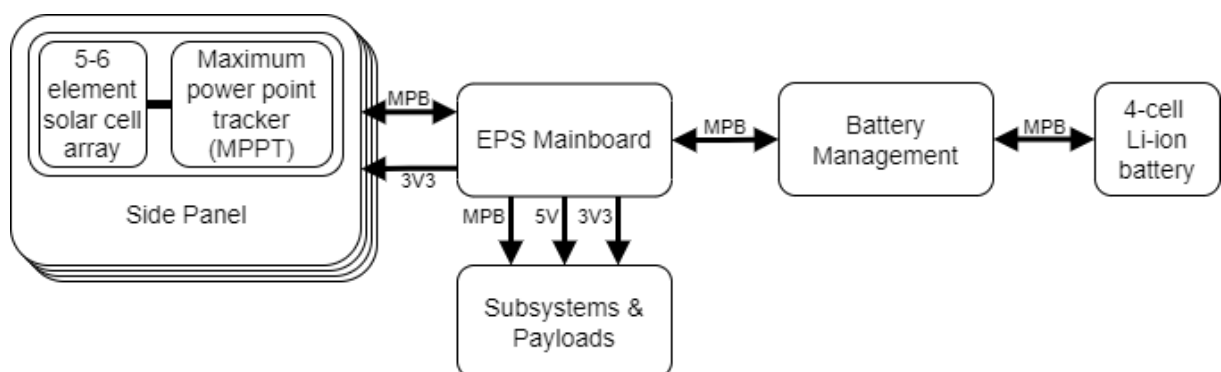
Figure 3.1. Diagram of power distribution system on ESTCube-2 satellite. Arrows show the flow of the energy.

The six side panels ´Printed circuit boards (PCBs) on-board the satellite, glued to the six sides, are responsible for many different tasks. However, one of the most important tasks for them is to provide harvested solar energy to the entire satellite and charge the Li-ion battery cells. This is done through the MPPT step-down converter that outputs harvested power to MPB.

Using the MPB, EPS provides power to itself and to the rest satellite's avionics module, consisting of the on-board computer, communications and the star tracker subsystems.

3.1 Solar panel's configuration
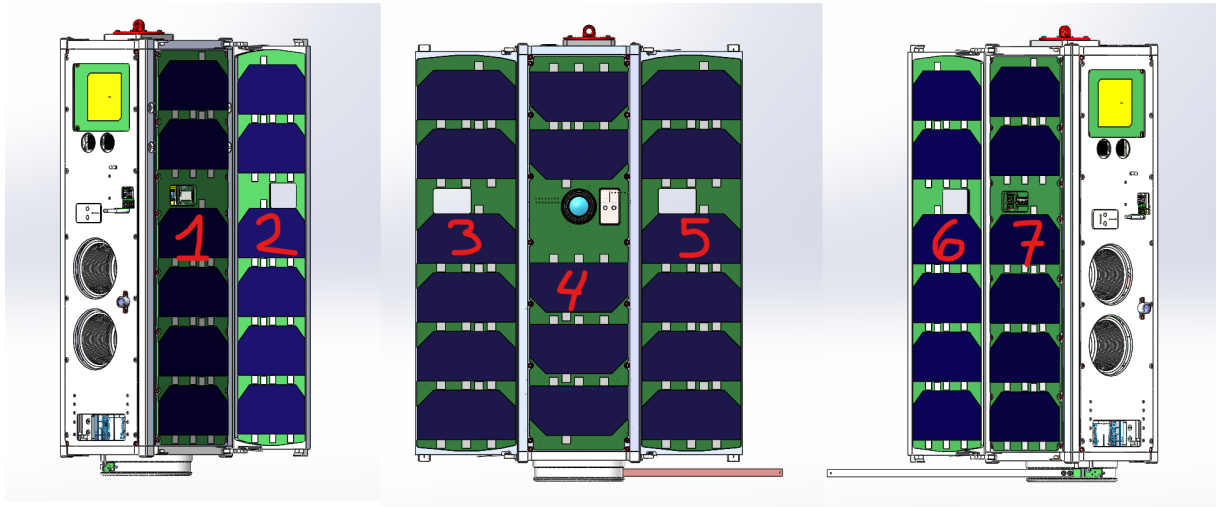
Figure 3.2. The ESTCube-2 solar panels configuration.

ESTCube-2 will have, in total, seven solar panels that will be covered with connected in series AzurSpace 3G30A solar cells. The solar panel configurations can be seen in figure 3.2 [25]. Panels numbered 2, 3, 5 and 6 are hosted on deployable wings. Other panels are attached to the primary satellite's body.

Each solar cell will be glued to an outer side panel PCB, which itself will be attached with adhesive to the satellite frame or a wing deployable. The solar cells are covered with cover glass to counteract radical oxygen that is present in LEO and to block UV radiation. Most solar panels except panel 4 will house six solar cells. The fourth panel of the spacecraft has five cells due to the size of the lens of the star tracker camera.

Each solar panel will be connected to its own power harvesting module allowing for independent control of the MPP.

The power production is mostly done by three panels, 3, 4 and 5, facing the sun directly. The other solar panels will be collecting power from the Earth's albedo, providing some power.

3.2 Overview of power harvesting system

The primary responsibility of the ESTCube-2 power harvesting subsystem is to obtain maximum power with the highest efficiency from the solar panels, thus providing power to all on-board systems and for charging the batteries. The centrepiece of the power harvesting subsystem is shown in the block diagram 3.3 initially created by Davis Fishers [26].
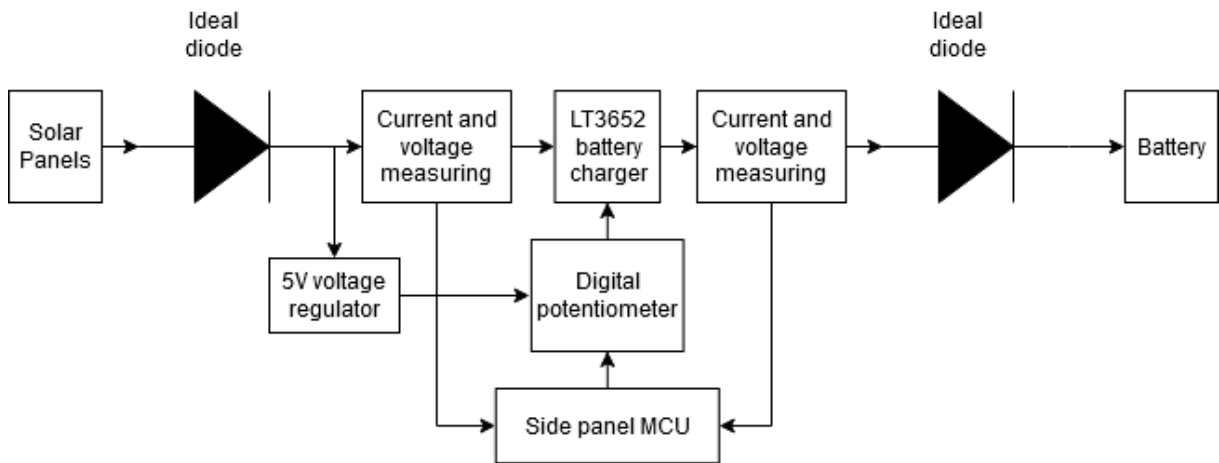
Figure 3.3. High level overview of the MPPT circuitry.

The system utilizes an LT3652 battery charger integrated circuit (IC) [27] with an adjustable reference voltage input responsible for controlling the charge current. If the reference voltage is increased so is the charge current and vice versa. This allows for the implementation of MCU based MPPT algorithms.

In order to control the voltage at the reference voltage input, a Microchip MCP4161 [28] digital potentiometer was added. A 5V low-dropout voltage regulator was added to supply the potentiometer. This approach was selected to have a direct supply from the solar panel in case of EPS' inability to supply a 5V which could lead to the power harvesting system malfunctioning. A vital factor for using a 5V voltage regulator is to have a larger regulation range, allowing for more precise input voltage control.
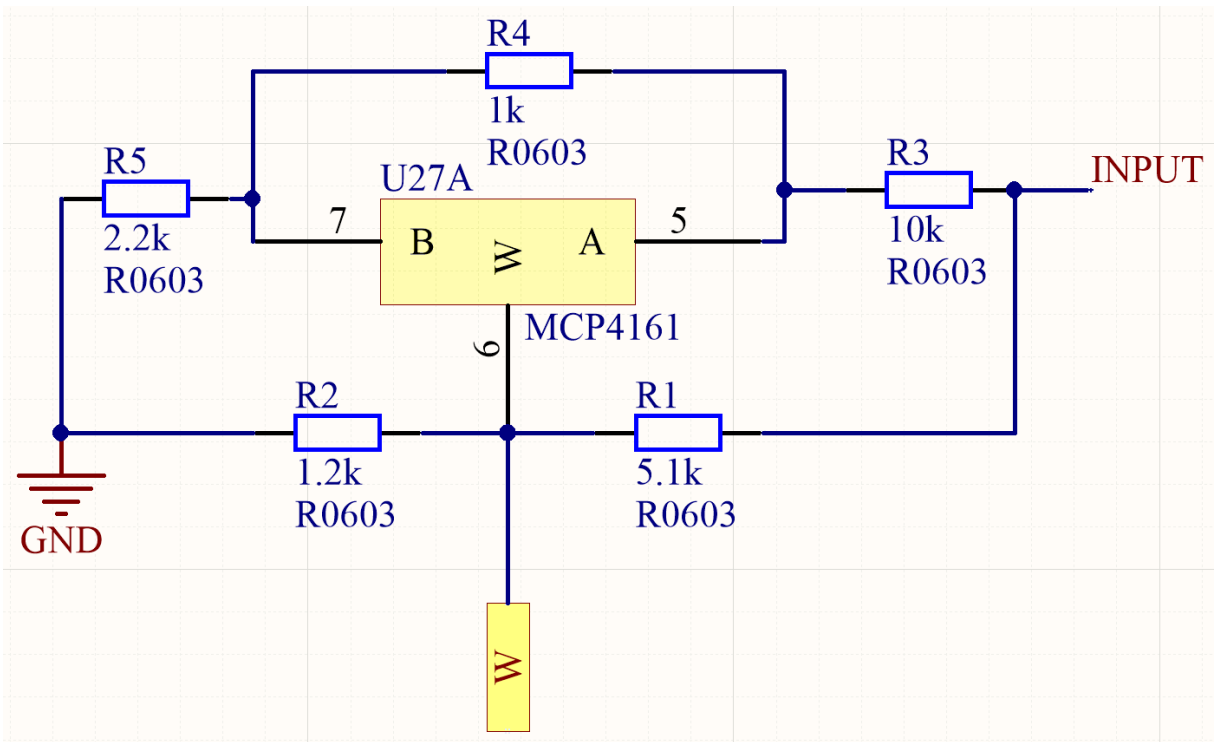
Figure 3.4. The resistor network structure for controlling reference voltage.

Figure 3.4 shows the configuration of the resistor network. The output from solar panels is connected to the digital potentiometer terminal A through resistor R3. The resistors around the digital potentiometer (R3, R4 and R5) are used to set the voltage to an appropriate voltage reference regulatory range and protect from overvoltage supply. The potentiometer wipers (W) output is then fed into the LT3652 battery chargers voltage reference pin.

Number of cells	Min - max voltage of solar cells	Min - max voltage of voltage divider	Panel number
6	12.28V - 16.14V	2.6V - 2.8V	1, 2, 3, 5, 6, 7
5	12.28V - 13.45V	2.6V - 2.8V	4

Table 3.1. The ESTCube-2 solar panel's configuration.

The power harvesting subsystem has two different configurations due to the varying amounts of solar cells on the satellite sides. The configuration can be changed by differing the values of resistors in the resistor network and the input voltage divider (R1 and R2) to change the voltage relationship. The configuration ranges for the potentiometer network can be seen in the table 3.1. The minimal voltage is set by the LT3652 battery charger minimum operating range, and the solar panel's open-circuit voltage sets the maximum voltage.

The power harvesting module uses two Linear Technology LT6105 [29] current-sense amplifiers for current measurements, along with two voltage dividers for input and output voltage measurements. The analogue outputs of those components are directly connected to the MCU's

internal ADC inputs. The measurements are used in the MPPT algorithm as well as for monitoring the power extraction efficiency.

Finally, in order to prevent backward current flow into the solar cells, there are two near-ideal diodes made by LTC4412 Low Loss PowerPath Controller [30] and SiA483DJ P-Channel 30 V MOSFET [31]. The diodes are located on the input and output of the power harvesting system.

The following list includes an overview of changes that have been made during this thesis by the author in order to fix problems of different MPPT hardware revisions.

- The supply voltage to LT6105 current-sense amplifiers was changed from 3.3V to 8.4V in order to allow a finer sensing of the change in current.

- The BOOST rectifying diode was incorrectly connected to the SENSE terminal on the LT3652 battery charger. The new revisions of the MPPT hardware fix this issue.

- The LT3652 battery charger input decoupling capacitor was moved closer to to chip in order to prevent voltage instability on VIN.

- The newer revisions implements a better component layout for the MPPT circuitry.

- To save physical space the SRR1240-150M inductor for the battery charger inductor sense resistor circuitry was changed to MSS7348 inductor that has a smaller footprint

3.3   Thesis goals

The goal of this thesis is to get the MPPT as close to flight ready as possible. To achieve this, the author, along with the ESTCube technical team, set the following goals:

- Create the needed hardware test setup for MPPT testing.

- To ease MPPT testing on the ground, the MPPT should have an easily accessible debug interface with a developers computer.

- The satellite operators must be able to obtain information about MPPT input and output current, input and output voltage, temperature of the MPPT charging circuitry and the estimated temperature of the solar panels.

- Information about the MPPT operational state shall be accessible to the satellite operators. This includes the currently used algorithm, MPPT faults and MPPT operational state.

- The MPPT should be able to provide power with an efficiency of at least 70 %. This replicates the efficiency of Arduino based MPPT solution made by previous ESTCube engineers.

- The duration of a MPPT tracking cycle shall be lower than 100 ms. The MPPT should be able to adjust the maximum power point at least ten times while the satellite is rotating at one revolution per second.

4 Implementation of MPPT algorithms

This chapter will focus on describing the implementation of different MPPT algorithms as well as used frameworks and tools in the process of developing the software. Due to the having the problems of testing the software in the actual sunlight, most of the software was mostly tested in-house using available tools at the laboratory.

4.1 Software Design

The final software consist of multiple layers which can be seen in figure 4.1 [25]. The ESTCube team uses firmware bundled in logical layers where each layer can talk with the one below it through API calls.
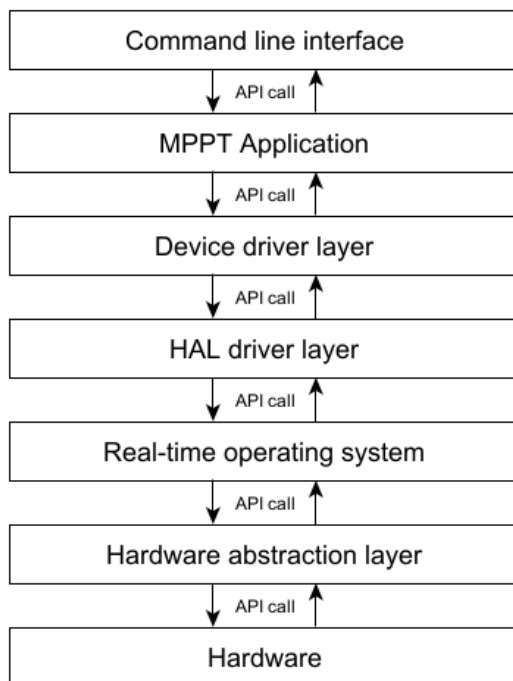
Figure 4.1. The MPPT software layers.

The following list provides a small description of every layer:

- **The Hardware Abstraction Layer (HAL)** hides the MCU specific details from the

35

higher software layers. This allows developers to develop software without knowing all the device specific details about the MCU functions.

- **A real-time operating system (RTOS)** is used to maximise the efficiency of an embedded system by implementing task synchronisation and multitasking capabilities while ensuring the real-timeliness of the entire system.

- **The HAL driver layer** acts as an arbiter between all the tasks by ensuring that requests to the peripherals are fulfilled in the order they are received.

- **The Device driver layer** is responsible for providing logic for controlling external devices attached to the MCU.

- **The MPPT application layer** is responsible for the logic that controls the finding and maintaining the maximum power point.

- **The Command Line Interface (CLI)**, not present in flight software, allows sending commands to the MPPT application layer using a developers computer. Therefore allowing for convenient control and debugging of MPPT software.

The main software layers that the author worked on are the device drivers, the MPPT and the command line interface (CLI). In order to control the potentiometer, which adjusts the voltage reference for the battery charging chip, the MCP4161 device driver was written. Additionally, the author created unit tests to verify the created device driver.

The software controlling the MPPT temperature sensor and battery charging chips, were already written by other team members. During the thesis the author updated the drivers to follow the latest ESTCube development. The primary development process took place in the created an MPPT application layer the creation of commands in the ESTCube CLI layer, that enables the user to log live data. Finally, the author fixed bugs that were found in the HAL layer during software development.

4.2   Maximum power point tracking

The algorithm development started by implementing four different algorithms: P&O, P&O with variable step size, IncCond and a temperature based power point tracking. However, this section mostly focuses on the P&O algorithm as it was chosen over the previously mentioned algorithms due to their implementation problems, low efficiency and the author's available time. Therefore in depth discussions about those algorithms is out of the scope of this thesis.

The logic of the MPPT software can be seen in figure 4.2. The MPPT software starts by initializing the needed peripheral devices such as the ADC, the digital potentiometer and the battery charger. The software then proceeds with the initialization of the actual MPPT layer, where a FreeRTOS task is created for power point tracking and the needed ADC channels are registered with the ADC driver with a sampling time of 1 ms.

Following the setup, the created FreeRTOS MPPT task starts measuring the input current and voltage to get the power that is being input into the system. The amount of measurements to average for the final input power value is specified in the MPPT layer configuration file which modifies the MPPT layer during compilation.

Next, the task calculates the produced power and both input and output power into a vector array which is then passed into to the currently active MPPT algorithm function. As mentioned before, there are several algorithms to choose from when tracking the maximum power point. However, only P&O has been successfully fine tuned to be in working order. The MPPT task can be reconfigured during runtime to switch to different maximum power point tracking algorithm.

Using the input values, the MPPT algorithm calculates the direction in which the resistance of the digital potentiometer needs to be changed in order to increase output power production. Using this information, the algorithm sends the appropriate command to the digital potentiometer so reference voltage could be perturbed in the direction of the MPP. After this step, the measurement cycle starts again and is continued endlessly.
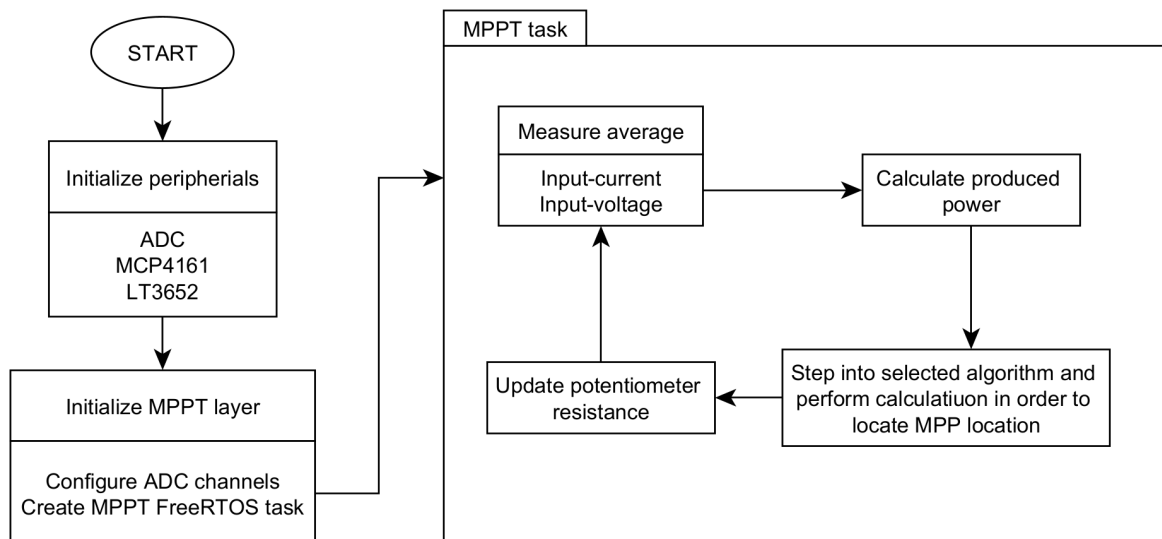
Figure 4.2. High-level software logic of MPPT.

4.3 Command line interface

The CLI layer enables a developer to configure the MPPT layer while it's running, and returns live telemetry of the MPPT. The CLI application layer uses the FreeRTOS CLI framework [32]. This enables a convenient way of creating various commands that control code execution by using a serial connection between a developers PC and a MCU. The author created various commands to speed up and ease the process of MPPT development and debugging. The following list gives the reader an overview of the most useful commands:

- **MPPT_SUSPEND** call suspends the running MPPT function by suspending the FreeRTOS task.

- **MPPT_RESUME** call resumes the MPPT layer FreeRTOS task.

- **MPPT_DATA** call returns currently produced telemetry of power production as well as the recent charging or fault states.

- **MPPT_PLOT** call is used to sweep through all digital potentiometer resistance values in order to display the location of MPP.

In addition to the CLI, a graphical user interface (GUI) was created using Python with PyQt graphic library. The GUI interface can be seen in figure 4.3. The GUI provides a straightforward way to monitor the MPPT telemetry. The GUI has two graphs, one of which depicts the resistance change over time, and the other displays produced input and output power. The right part of the interface shows latest live values received over via the serial port connection.

The GUI interface was able to display necessary data, which helped the author to speed up the process of algorithm development as well as to log essential data during test MPPT procedures.
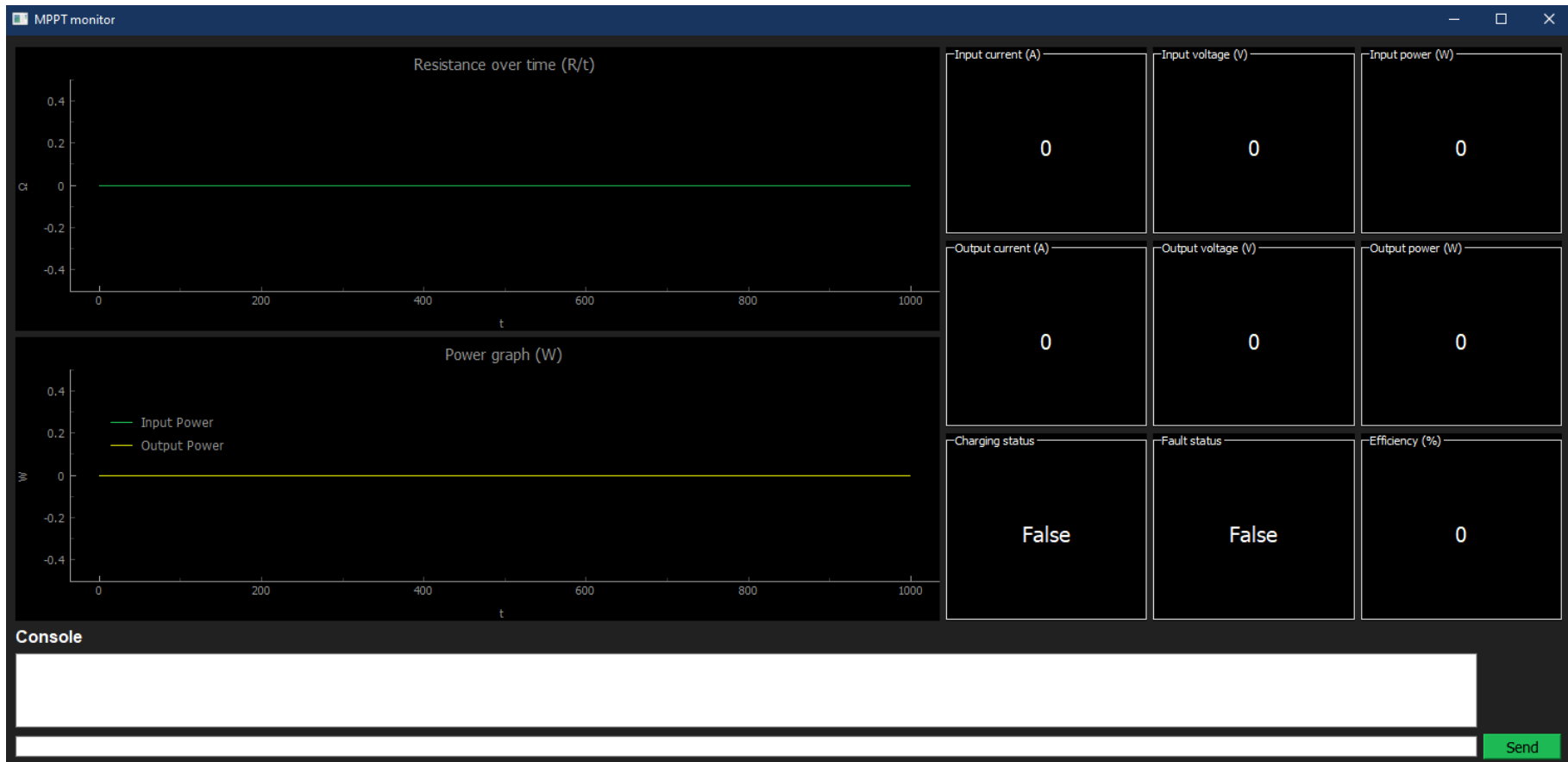
Figure 4.3. The MPPT GUI interface.

5 Testing

This chapter contains the results of the software and hardware testing as well as an explanation of how the tests were conducted.

5.1 SMU testing

The first tests were conducted via a source and measuring unit (SMU) that is capable of both sourcing current and measuring voltage, simultaneously. The SMU used the LUA scripting language, allowing for the creation of different test scenarios. The testing algorithm were created using mathematical expressions describing the behaviour of solar cells. The mathematical terms were based on Geoffrey Walker's Matlab model [12], and the full script implementation can be seen in appendix II.
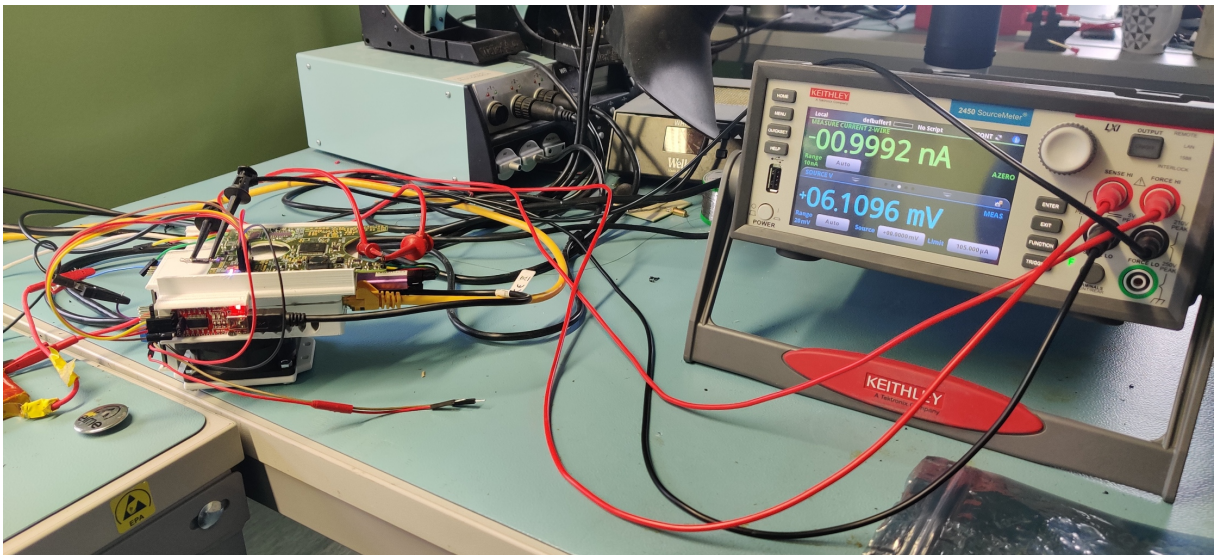
Figure 5.1. The SMU testing setup for P&O algorithm

The SMU testing results are shown in figure 5.2. In total two tests has been made The left part of the figure shows the MPPT work with different incidence angles simulated by an SMU script. The angles started from 0 degrees (directly facing the Sun) and were incremented by 15 degrees until an angle of 90 degrees was reached (perpendicular to the Sun). Each angle
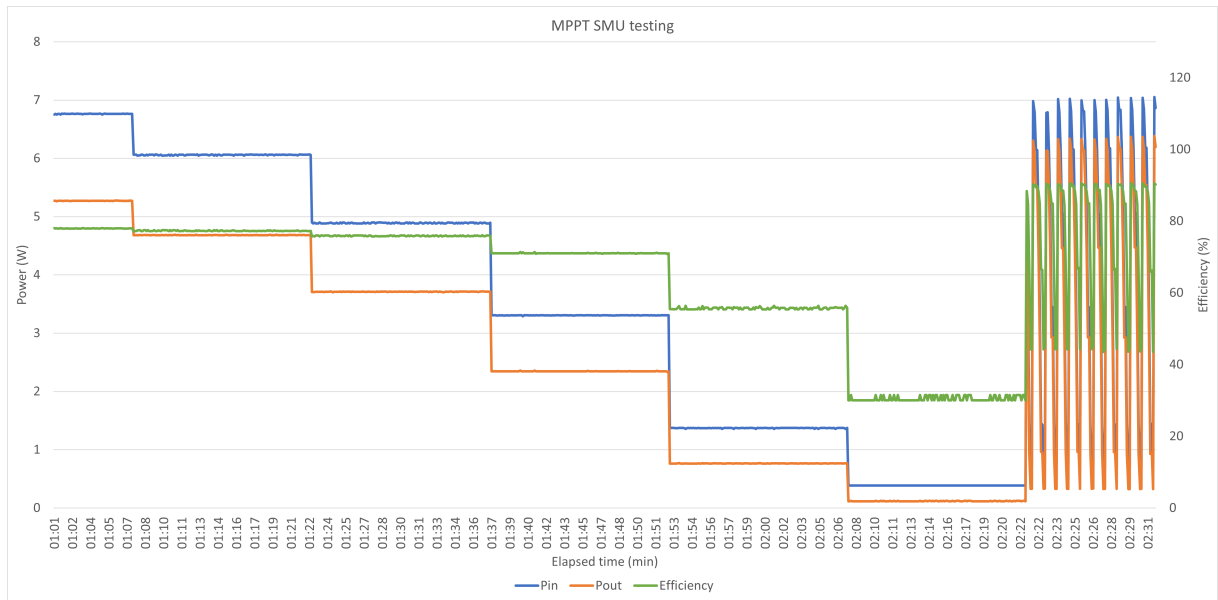
Figure 5.2. The results of SMU testing.

was set for 15 seconds to produce an estimated power level that the actual solar cell would do. As can be seen, the efficiency at higher power production levels 7.2 W to 4.9 W the algorithm kept the efficiency of 75-79%. However, the algorithm started dropping its efficiency when power production dropped below 4W and proceeded. The author suggests that the I-V curve has started to flatten, and P&O could not track the MPP efficiently. The right part of the figure emulates the satellite's rotation at a speed of one revolution per second. A mean efficiency of 78% was achieved during this test. However, there is a concern that the algorithm can't keep up the efficiency at higher angle speed changes, so this issue needs to be researched more.

5.2   MPPT testing in sunlight

In order to test the solar power harvesting system in the actual sunlight, a test bench was created. The testing setup consisted of 6 AzurSpace 3G30A mechanicals type cells [33] connected in series. Mechanicals are cheaper variant of the real solar cells but they have minor defects. The output of the created solar panel was directly connected to an old revision of the fourth solar panel PCB. The PCB was connected to a Raspberry Pi host computer allowing for software debugging.

The communication with a MPPT was enabled by an FTDI FL232RT [34] UART interface. The interface was plugged into the Raspberry Pi USB port, and the other end was connected with the MCU UART peripheral through dupont wires.

Figures 5.3 and 5.4 give the reader an overview of the created setup and how the different

41

components of it were connected with each other.
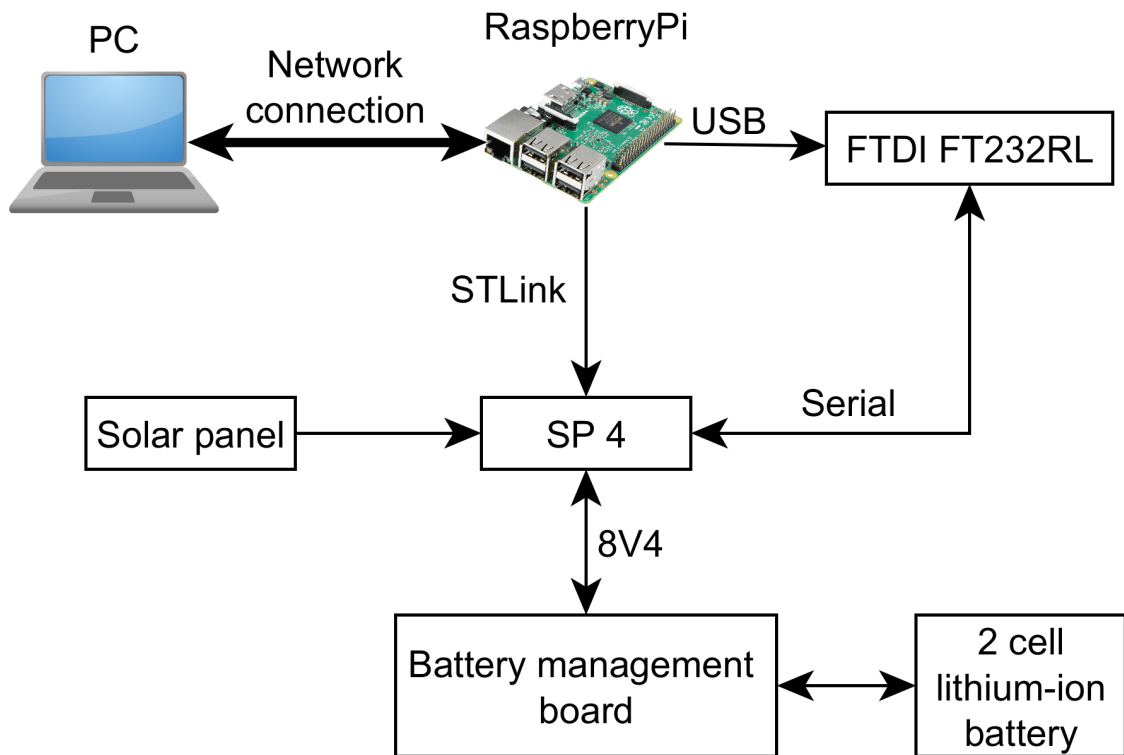
Figure 5.3. The block diagram of testbench configuration.

During the testing, different types of loads were used to simulate the satellite: a programmable 150 W electronic load, a 2-cell (2s) Lithium-ion Panasonic NCA103450 [35] battery and a combination of both. Both loads were connected to the MPB. The main difference was the battery being connected to MPB through a battery management board for balancing and protection purposes.
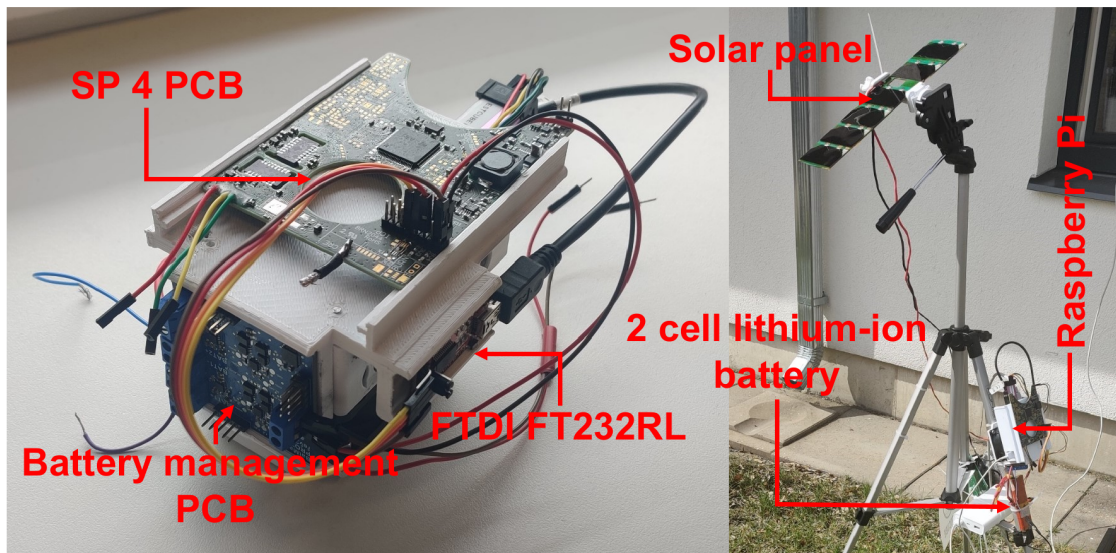
Figure 5.4. The image of testbench configuration.

Unfortunately, the SMU test results could not be replicated and the the final efficiency of the MPPT in the actual sunlight is approximately 60% at full illumination. Due to problems with data saving, the results of the testing were lost.

The probable cause of slightly dropped efficiency can be the state of damaged solar cells. In addition, the high peak to peak voltage of 500 mV to 1 V has been discovered during the testing of MPPT circuitry, which also could cause performance issues. Another hypothesis may be a wrongly configured resistor network around the digital potentiometer, that sets inappropriate adjustment range of reference voltage.

In order to achieve better results, the author proposed the following solutions in order to fix underperformance issues.

- Recalculate values for the resistor network.

- Reduce the peak to peak voltage by adding additional capacitors close to the input of LT3652 battery charger IC.

- Recheck testing setup in order to find connection issues.

- Re-examine ADC accuracy in sensing input current and input voltage.

6 Conclusions and future work

During the thesis, the author implemented a working prototype of MPPT on the ESTCube-2 hardware. The thesis covered work on the development of software and described the conducted tests in order to test the work of the MPPT algorithm.

The final implementation achieved an efficiency of around 75% to 79% at higher power production levels. However, the algorithm could not maintain steady efficiency at lower power production levels. Another issue is that the algorithm could not keep the steady efficiency at a speed of one revolution per second. Finally, the author managed to find some hardware issues in the previous revision of the MPPT and has either suggested or applied the according fixes.

Most of the requirements were met except achieving the response time from the algorithm of one revolution per second, which is an important hard requirement for ESTCube-2.

In the future, the MPPT software should be tested with the new side panel PCBs and other implemented algorithms. Due to the structure of created software, the software can be easily expanded in the future. Many implemented algorithms have not been adequately tested, such as variable step size P&O and Incremental conductance; therefore, future work will focus on tests of those algorithms.

Bibliography

[1] Osisioma Ezinwanne, Fu Zhongwen, and Li Zhijun. „Energy Performance and Cost Comparison of MPPT Techniques for Photovoltaics and other Applications". In: *Energy Procedia* 107 (2017), pp. 297–303. ISSN: 1876-6102. DOI: `https://doi.org/10.1016/j.egypro.2016.12.156`. URL: `https://www.sciencedirect.com/science/article/pii/S1876610216317453` (visited on 22/10/2021).

[2] David Pignatelli and A Mehrparvar. „CubeSat Design Specifications Rev. 14". In: *The CubeSat Program, Cal Poly SLO* (2020). Publisher: California Polytechnic State Univ. San Luis Obispo, CA (visited on. 4/10/2021).

[3] Iaroslav Iakubivskyi et al. „Coulomb drag propulsion experiments of ESTCube-2 and FORESAIL-1". In: *Acta Astronautica* 177 (2020), pp. 771–783. ISSN: 0094-5765. DOI: `https://doi.org/10.1016/j.actaastro.2019.11.030`. URL: `https://www.sciencedirect.com/science/article/pii/S0094576519314250` (visited on 28/12/2021).

[4] Yael Kovo. *State of the Art of Small Spacecraft Technology*. Publication Title: NASA. June 2020. URL: `https://www.nasa.gov/smallsat-institute/sst-soa-2020` (visited on 5/10/2021).

[5] *Voyager - Radioisotope Thermoelectric Generators (RTG)*. Publication Title: NASA. URL: `https://voyager.jpl.nasa.gov/mission/spacecraft/instruments/rtg/` (visited on 22/10/2021).

[6] Marvin Warshay and Paul R Prokopius. *The fuel cell in space: yesterday, today and tomorrow*. Lewis Research Center, 1989 (visited on. 22/10/2021).

[7] E. Werthheimer, L. Berthoud, and M. Johnson. *PocketRTG – a CubeSat Scale Radioisotope thermoelectric generator using COTS fuel*. 2015 iCubeSat Workshop, London, U.K., May 2015 (visited on. 4/1/2022).

[8]   Ferdaous Masmoudi, Fatma Ben Salem, and Nabil Derbel. „Identification of internal parameters of a mono-crystalline photovoltaic cell models and experimental ascertainment". In: *International Journal of Renewable Energy Research* 4 (Jan. 2014), pp. 840–848 (visited on. 30/12/2021).

[9]   Afshin Izadian, Arash Pourtaherian, and Sarasadat Motahari. „Basic model and governing equation of solar cells used in power and control applications". In: *2012 IEEE Energy Conversion Congress and Exposition (ECCE)*. 2012, pp. 1483–1488. DOI: `10.1109/ECCE.2012.6342639` (visited on. 31/12/2021).

[10]   Mohammed R. AlRashidi, K. M. El-Naggar, and Mohamad F. AlHajri. „Parameters Estimation of Double Diode Solar Cell Model". In: *International Journal of Electrical and Computer Engineering* 7 (2013), pp. 118–121 (visited on. 30/12/2021).

[11]   *TJ Solar Cell 3G30C Datasheet*. URL: `http://www.azurspace.com/images/0003429-01-01_DB_3G30C-Advanced.pdf` (visited on 22/10/2021).

[12]   Geoffrey Walker. „Evaluating MPPT converter topologies using a Matlab PV Model". In: *Journal of Electrical and Electronics Engineering, Australia* 21 (Jan. 2001) (visited on. 4/5/2022).

[13]   Boualem Bendib, Hocine Belmili, and Fateh Krim. „A survey of the most used MPPT methods: Conventional and advanced algorithms applied for photovoltaic systems". In: *Renewable and Sustainable Energy Reviews* 45 (2015), pp. 637–648. ISSN: 1364-0321. DOI: `https://doi.org/10.1016/j.rser.2015.02.009`. URL: `https://www.sciencedirect.com/science/article/pii/S1364032115000970` (visited on 24/11/2021).

[14]   A. Rezaee Jordehi. „Maximum power point tracking in photovoltaic (PV) systems: A review of different approaches". In: *Renewable and Sustainable Energy Reviews* 65 (2016), pp. 1127–1138. ISSN: 1364-0321. DOI: `https://doi.org/10.1016/j.rser.2016.07.053`. URL: `https://www.sciencedirect.com/science/article/pii/S1364032116303811` (visited on 11/10/2021).

[15]   *MPPT algorithm*. Publication Title: MathWorks. URL: `https://uk.mathworks.com/solutions/power-electronics-control/mppt-algorithm.html` (visited on 24/11/2021).

[16] Fan Zhang et al. „Adaptive hybrid maximum power point tracking method for a photovoltaic system". In: *IEEE Transactions on Energy Conversion* 28.2 (2013). Publisher: IEEE, pp. 353–360 (visited on. 24/10/2021).

[17] Ömer Faruk TOZLU and Hüseyin ÇALIK. „A Review and Classification of Most Used MPPT Algorithms for Photovoltaic Systems". In: *Hittite Journal of Science and Engineering* 8.3 (), pp. 207–220 (visited on. 10/11/2021).

[18] Nevzat Onat. „Recent developments in maximum power point tracking technologies for photovoltaic systems". In: *International Journal of Photoenergy* 2010 (2010). Publisher: Hindawi (visited on. 9/11/2021).

[19] Mihkel Pajusalu et al. „Design and pre-flight testing of the electrical power system for the ESTCube-1 nanosatellite". In: *Proceedings of the Estonian Academy of Sciences* 63.2 (2014). Publisher: Teaduste Akadeemia Kirjastus (Estonian Academy Publishers), p. 232 (visited on. 28/9/2021).

[20] M. Pajusalu et al. „Analysis of the electrical power system for ESTCube-1". In: *Proceedings of the International Astronautical Congress, IAC* 9 (Jan. 2013), pp. 6794–6798 (visited on. 10/11/2021).

[21] Andrew E. Kalman. *"Pumpkin's Colony I CubeSat Bus: Past, Present and Future," GAINSTAM (Government And Industry Nano-Satellite Technology And Mission) Workshop*. Huntington, Beach, CA, USA, Nov. 2009. URL: http://www.cubesatkit.com/docs/press/Pumpkin_GAINSTAM_2009.pdf (visited on 24/11/2021).

[22] Stephen Arnold et al. „QbX-the CubeSat experiment". In: (2012) (visited on. 23/10/2021).

[23] Jussi Hemmo. „Electrical Power Systems for Finnish Nanosatellites". English. MA thesis. Aalto University. School of Electrical Engineering, 2013. URL: http://urn.fi/URN:NBN:fi:aalto-201401141129 (visited on 11/10/2021).

[24] M. Rizwan Mughal et al. „Aalto-1, multi-payload CubeSat: In-orbit results and lessons learned". In: *Acta Astronautica* 187 (2021), pp. 557–568. ISSN: 0094-5765. DOI: https://doi.org/10.1016/j.actaastro.2020.11.044. URL: https://www.sciencedirect.com/science/article/pii/S0094576520307190 (visited on 12/1/2022).

[25] *ESTCube-2 Software structure*. Unpublished internal ESTCube document. (visited on. 10/5/2022).

[26] Dāvis Fišers. „NANOSATELĪTA ESTCUBE-2 FUNKCIONĀLO MODUĻU INTEGRĀCIJA SĀNU PANEĻOS". PhD thesis. Ventspils Augstskola, 2020 (visited on. 10/5/2022).

[27] *LT3652 - Power tracking 2A battery charger for Solar Power*. Publication Title: www.analog.com. URL: `https://www.analog.com/media/en/technical-documentation/data-sheets/3652fe.pdf` (visited on 22/4/2022).

[28] *7/8-bit single/dual SPI digital POT*. URL: `https://ww1.microchip.com/downloads/en/DeviceDoc/22059b.pdf` (visited on 22/4/2022).

[29] *LT6105 - Current Sense Amplifier*. Publication Title: www.analog.com. URL: `https://www.analog.com/media/en/technical-documentation/data-sheets/6105fa.pdf` (visited on 22/4/2022).

[30] *LTC4412 - Low Loss PowerPath™ Controller in ThinSOT*. Publication Title: www.analog.com. URL: `https://www.analog.com/media/en/technical-documentation/data-sheets/ltc4412.pdf` (visited on 16/5/2022).

[31] *SiA483DJ - P-Channel 30 V (D-S) MOSFET*. Publication Title: www.vishay.com. URL: `https://www.vishay.com/docs/62779/sia483dj.pdf` (visited on 16/5/2022).

[32] *FreeRTOS+CLI*. URL: `https://www.freertos.org/FreeRTOS-Plus/FreeRTOS_Plus_CLI/FreeRTOS_Plus_Command_Line_Interface.html` (visited on 19/5/2022).

[33] *TJ Solar Cell 3G30A Datasheet*. URL: `http://www.azurspace.com/images/products/0003401-01-01_DB_3G30A.pdf` (visited on 4/5/2022).

[34] *FT232R USB UART IC Datasheet*. URL: `https://ftdichip.com/wp-content/uploads/2020/08/DS_FT232R.pdf` (visited on 10/5/2022).

[35] *NCA103450 PANASONIC*. URL: `https://www.tme.eu/Document/9e900482d561b2729 NCA103450.pdf` (visited on 12/5/2022).

Acknowledgements

I want to thank my family members and the people who surrounded me during my studies. Especially, I would thank Janis Dalbins and Kristo Allaje, who supervised me through this adventure. Finally, I would like to thank Kristo for taking away my last cigarette.

Appendices

I MPPT Software

Due to the software being an intellectual property of the Estonian Student Satellite Foundation, a copy of the software can be requested by contacting the ESTCube team at estcube@estcube.eu.

II SMU Script

```
--Reset the instrument
reset()
defbuffer1.clear()


--Source Settings
smu.source.func = smu.FUNC_DC_CURRENT
smu.source.vlimit.level = 16.140
smu.source.level = 0


--Measure Settings
smu.measure.func = smu.FUNC_DC_VOLTAGE
smu.measure.nplc = 0.01
smu.measure.sense=smu.SENSE_4WIRE


function AzurSpace(Va, insolation ,TaC,Ns,Iang)
  -- Va = array voltage
    -- Ia = array current
  -- insolation = solar radiation energy on a given surface area (AM0=1367W
     /m2)
  -- TaC = Temperature in Celsius degrees
  -- Ns = number of series connected cells (diodes)


  --variables
  k = 1.38*(10^(-23)) -- Boltzmann's constant
  q = 1.602*(10^(-19)) -- Charge of an electron
  Tref = 273 + 28 -- reference temperature
  Voc_T1 = 2.69 -- Open Circuit voltage @ T=28C
  Isc_T1 = 0.5196 -- Short Circuit current @ T=28C


  -- "diode quality" factor, =2 for crystaline, <2 for amorphous, chosen to
  -- fit the curve
  n = 1.5
  -- Band gap voltage, 1.12eV for xtal Si, ?1.75 for amorphous Si.
  -- Source for chosen value: Architectural Design Criteria for Spacecraft
     Solar Arrays
  Vg = 1.42


  -- Temperature in Kelvins
```

```lua
    TaK = 273 + TaC
    -- insolation in Watts/m2
    insolation = insolation / 1367
    -- Iph at reference temperature
    Iph_T1 = Isc_T1 * insolation
    -- Change in Iph per degree
    a = 0.28e-3/Isc_T1
    -- Photogenerated current Iph at selected temperature
    Iph = Iph_T1 * (1 + a * (TaK - Tref))
    -- =A*kT/q
    Vt_T1 = (k*Tref)/q
    -- Diode saturation current of Diode 2 at T=28C
    Id_T1 = Isc_T1 / (math.exp(Voc_T1/(n*Vt_T1))-1)
    b = Vg * q /(n*k)
    -- Diode saturation current at selected temp
    Id = Id_T1 * (TaK/Tref)^(3/n) * math.exp(-b *(1/TaK - 1/Tref))
    -- Chosen to match the curve
    Rs = 0.304
    -- =n*kT/q
    Vt_Ta = (n*k*Tref)/q
    -- Measured voltage / Number of cells
    Vc = Va/Ns


    --calculates the current depending of the voltage
    I = Iang - (Iph - Iang - Id * (math.exp((Vc+Iang*Rs)/Vt_Ta)-1)) / (-1 - (
        Id *(math.exp((Vc+Iang*Rs)/Vt_Ta)-1))*Rs/Vt_Ta)


    return I
end


--variables
Isc_T1 = 0.5196 -- Short Circuit current @ T=28C
n_cells = 6
time_to_run = 60 -- Each intensity
iterator = 1
temp = 28
I = Isc_T1


-- Calculated solar intensities depending on the incidence angle of Sun W/m
    ^2 with cover glass loss
```

```lua
-- Incidence angles = 0, 15, 30, 45, 60, 75, 90
intensities = {1307, 1262, 1130, 914, 619, 262, 0}


smu.source.output = smu.ON              --turns on output of the SMU


timer.cleartime()
first_dt = timer.gettime()
while true do
  Volt = smu.measure.read(defbuffer1)       --reads voltage


  value = intensities[1]
  I = AzurSpace(Volt, value, temp, n_cells, I) --intensities[1]
  print(I)


  if I <= 0.05 then           --script has problems operating when currrent is
      close to 0 soo this prevents dropping current to zero
    I=0.05
  end


  smu.source.level = I        -- changes the current output value of the SMU


  difference = timer.gettime() - first_dt
  -- change intensiti
  if (difference > time_to_run) then
    -- #intensities if table.getn(intensities) throws error table.getn was
        deprecated in 5.1 and removed in 5.2.
    if (table.getn(intensities) > iterator) then
      iterator = 1 + iterator
    else
      iterator = 1
    end


    first_dt = timer.gettime()
  end
end
```

Licence

Non-exclusive licence to reproduce the thesis and make the thesis public

I, **Kirill Anohin**,

1. grant the University of Tartu a free permit (non-exclusive licence) to

   reproduce, for the purpose of preservation, including for adding to the DSpace digital archives until the expiry of the term of copyright, my thesis

   "Development of Maximum Power Point Tracking for ESTCube-2"

   supervised by Janis Dalbins and Kristo Allaje

2. I grant the University of Tartu a permit to make the thesis specified in point 1 available to the public via the web environment of the University of Tartu, including via the DSpace digital archives, under the Creative Commons licence CC BY NC ND 4.0, which allows, by giving appropriate credit to the author, to reproduce, distribute the work and communicate it to the public, and prohibits the creation of derivative works and any commercial use of the work until the expiry of the term of copyright.

3. I am aware of the fact that the author retains the rights specified in points 1 and 2.

4. I confirm that granting the non-exclusive licence does not infringe other persons' intellectual property rights or rights arising from the personal data protection legislation.

Kirill Anohin

20.05.2022